NASA TECHNICAL TRANSLATION NASA TT-20161

III-34
141231
308

DESIGNS OF PROFILES FOR CASCADES

L. Goettsching

Translation of "Profilentwurf fuer Gitter".

Stuttgart University (West Germany). Inst. fuer Aeround Gasdynamik. in its Thermodynamic and Flow Mechanical Problems in Aircraft and Spacecraft Drives. April, 1986. pp 243-267. Report ETN-87-93751

(NASA-TT-20161) DESIGNS OF PROFILES FOR CASCADES (NASA) 30 p CSCL 20D

N88-22326

Unclas
G5/34 0141231

NATIONAL AERONAUTICS AND SPACE ADMINISTRATION
WASHINGTON D.C. 20546 APRIL 1988

NASA National Aeronautics and Space Administration

Report Documentation Page

1. Report No.	2. Government Accession No.	3. Recipient's Catalog No.
NASA TT-20161		

4. Title and Subtitle	5. Report Date
DESIGNS OF PROFILES FOR CASCADES	APRIL 1988
	6. Performing Organization Code

7. Author(s)	8. Performing Organization Report No.
L. GOETTSCHING	ETN-87-98751
	10. Work Unit No.

9. Performing Organization Name and Address	11. Contract or Grant No.
NATIONAL AERONAUTICS AND SPACE ADMINISTRATION WASHINGTON, DC 20546	NASW-4307
	13. Type of Report and Period Covered
12. Sponsoring Agency Name and Address	translation
NATIONAL AERONAUTICS AND SPACE ADMINISTRATION WASHINGTON, DC 20546	14. Sponsoring Agency Code

15. Supplementary Notes

Transl. from GERMAN into ENGLISH of "Profilentwurf fuer gitter," Inst. fuer Aeround Gasdynamik. in its Thermodynamic and Flow Mechanical Problems in Aircraft and Spacecraft Drives. Stuttgart University, West Germany. April 1986, pp 243-267. 87N14340

16. Abstract

Optimized cascade profiles for arbitrary applications were designed. The influence of Mach number, Reynolds number and degree of turbulence were taken into account. The optimization aimed at maximum pressure increase, maximum pressure loss, low Reynolds number dependence, or large angle-of-attack range. Starting from the boundary layer form parameter distribution (by which transition point and seaparation point can be controlled) the velocity distribution and the contour were calculated. The profile characteristics were tested off-design and were improved. Interferometric measurements were performed in the transonic cascade channel.

17. Key Words (Suggested by Author(s))	18. Distribution Statement
	unclassified-unlimited

19. Security Classif. (of this report)	20. Security Classif. (of this page)	21. No. of pages	22. Price
unclassified	unclassified	30	

NASA FORM 1626 OCT 86

Design of profiles for cascades* (Project B6)

/243**

1. Summary

The result of the work done in Project B6 is the design of optimized cascade profiles for any given applications. The influence of the Mach number, the Reynolds number and the degree of turbulence has been taken into account. The optimization was carried out with certain design objectives, e.g. maximum pressure increase, minimum pressure loss, low Reynolds number dependence, or large angle-of-attack range.

On the basis of the boundary layer form parameter distribution, by means of which the transition point and the separation point can be controlled, first of all the velocity distribution is calculated, and then, by means of inverse methods, the contour is calculated. Then the profile characteristics are tested "off-design" and improved if necessary.
Finally, experimental testing is done by means of interferometric measurements in the transsonic channel.

2. Introduction

The aerodynamic properties of a profile are mainly determined by the boundary layer development. Logically, the profile design begins with the determination of the boundary layer form parameter distribution.
From this is determined, by means of an inverse boundary layer program, the relevant boundary layer-optimized velocity distribution (chapter 3).
Using a design program (chapter 4), the profile contour is then calculated. In the case of transsonic flows the contour is calculated in conjunction with Project. B8.
After calculation of the profile contour, the velocity distribu-

---

* By L. Goettsching

**Numbers in margin indicate foreign pagination.

tions are determined using a follow-up computer program and the losses outside the design point are determined using a boundary layer program (chapter 5). /244

In order to assess the non-stationary effects produced by the relative movement between the wheel and the guide ring, a computer program was developed that can be used to calculated the non-stationary pressure distribution for frictionless flow (chapter 6).

The transsonic cascade channel was adapted for experimental testing and the illumination time for double-illumination holography was reduced mechanically to a few microseconds, so that detached flows can also be evaluated interferometrically (chapter 7).

3. Velocity optimization

The velocity distribution or the corresponding pressure distribution determines the thrust and the moment, while the resistance of the profile depends on the boundary layer development. The boundary layer form parameters are the determining factors for the wall thrust stress, the transition, the separation and re-attachment. Therefore it is much simpler to begin the profile optimization with the determination of the form parameter distribution.

3.1 Form parameter distribution

The form parameter distribution H32(s) is prescribed in four zones (Fig. 4).

In the laminar obstruction point zone $0 < s < sl$ with a constant velocity gradient, H32 = 1.625.

Next comes the laminar transition zone $sl < s < su$, with the transition at the point su. The form parameter should be selected according to the condition $R\delta 2(su) = R\delta 2_u(Tu, H32)$.

Figure 5 shows the transition Reynolds number in relation to the degree of turbulence and the form parameter.

In the turbulent transition zone $su < s < st$ usually a constant velocity $(H32 = H32(R\delta 2) \approx 1.75)$ or a slight velocity decrease is selected.

The maximum velocity, the thrust, the moment and the detachment behavior can be controlled by the selection of st. As st increases, the maximum velocity decreases and the nose-heavy moment increases, while the thrust reaches a maximum at a certain value of st. /245

If st is at 70% to 80% of the profile depth, when the angle of attack increases the separation point can only move up as far as st. As a result of the flap-like effect of the detached flow, the suction peak at the nose of the profile is reduced , so that leading edge separation can be avoided over a large angle-of-attack range /3/.

The turbulent terminal zone st < s < c is of decisive importance for the profile characteristics, as it controls the start of the turbulent separation.

Constant form parameters cause an abrupt migration of the separation point as far as st, while a decreasing form parameter H32 causes an earlier establishment with a constant migration of the separation.

3.2 Turbulent pressure increase

In order to make clear how much pressure increase a turbulent boundary layer can tolerate, how large the impulse loss is and whether there is an optimal turbulent pressure increase with low losses for a large pressure increase, Fig. 1 shows the equilibrium boundary layers with a constant form parameter.

As initial values, for 1% of the profile depth the impulse loss density $\delta 2/c = 0.0005$ and the velocity $U/U_\infty = 1.$ are given.

As can be expected, the impulse loss and the pressure increase are intensified with decreasing form parameter. However, the rear edge velocity again increases slightly close to separation (H32 < 1.54), with a simultaneous increases in losses.

The reason for the velocity increase is the simultaneously decreasing initial form parameter $H32_0$. If the initial form parameter remains constant, the rear edge velocity decreases continuously until separation occurs.

Older studies /9/ gave much lower losses and pressure increases. /246

Normally, before the onset of the pressure increase there is a turbulent equal pressure flow (H32 = 1.70 + 1.80).

For this case Stratford /8/ has studied empirically velocity distributions close to separation; these can be modified in a simple way in order to obtain distributions less in danger of separation. To do this, the initial impulse loss density is fictionally increased by multiplication by a parameter P.

Figure 2 shows the relation of the rear edge form parameter H32c to P.

With the exception of the initial form parameter $H32_0 = 1.8$, the same initial conditions were chosen as in the case of equilibrium distributions.

The original Stratford distribution with P = 1 is conservative relative to separation, since separation occurs only when $P < 0.77$ at the rear edge. When $H32_0 = 1.70$ the separation limit is already at P = 0.83.

The rear edge form parameter is only slightly dependent on the initial impulse loss density . In the case P = 1, the tenfold density of $H32_0 = 1.570$ produces 1.566, while one tenth of the initial density produces the value 1.578.

In addition, asymptotic equilibrium distributions were studied for the form $u \sim (s-s0)^m$. For s >> s0 the form parameter H32 only depends on the exponent m /10/.

The calculated impulse loss densities and rear edge velocities are no different from those shown in diagrammatic form in Fig. 1.

In Fig. 3 the distributions are compared for the same rear edge velocity. The somewhat greater velocity gradient at the beginning produces in the case of the Stratford distribution the lowest losses with the least tendency to separate. The following table gives the calculated values at the rear edge.

[1] Geschwindigkeitsverteilung	u_c/u_∞	$\Delta\Phi/u_\infty/c$	H32c	$\delta 2c/c*100$
Stratford P = 1	0.447	0.562	1.570	1.37
asympt. Aequilibrium m=-.242	0.447	0.567	1.558	1.48
Aequilibrium	0.447	0.565	1.540	1.67

Key: 1 velocity distribution.

The inverse boundary layer program calculates for any form parameter /247
distributions the relevant velocity distribution. A linear and a parabolic distribution of the third magnitude were studied. In comparison with equilibrium distributions, this produced, for the same rear edge velocity, much higher losses and a greater potential difference.

$H32_0$ = 1.70 was chosen as the initial parameter.

[1] Formparametervertailung	Uc/U∞	Δϕ/U∞/c	H32c	δ2c/c*100
linear (H32 =1.70 ÷ 1.52)	0.482	0.659	1.520	1.33
a. Aequilibrium m=-.231	0.482	0.602	1.616	1.07
[2]kub.Parabel(H32 =1.70 ÷ 1.52)	0.539	0.738	1.520	1.04
a. Aequilibrium m=-.212	0.539	0.655	1.669	0.76

Key: 1 form parameter distribution; 2 cub. parabola.

When calculating the velocity distribution from the form parameter distribution, the velocity gradient should be calculated iteratively at each connection point. Thus it is more favorable to give velocity distributions that depend on two parameters, so that the form parameter distribution and the rear edge form parameter can be pre-determined.
For this the exponential pressure distribution

$$cp = 1-(U/Ut)^2 = a*(s/c-st/c)^b \ .$$

is useful. So that the flow is close, $b \geqslant 1/3$ should be chosen.

Since $H32_0$ depends on the parameters a and b as well as the initial impulse loss density, instead of a the value F from the Stratford separation criterion /9/ is prescribed.

$$F=(2\cdot\bar{c}\mu_c)^{\frac{n-2}{4}}\cdot\sqrt{\bar{x}_c\cdot\bar{cp}_c'}\cdot\left(\frac{Re_{xc-}}{10^6}\right)^{-0.1}$$

In this way $H32_0$ can be give as a function of F with only a very slight dependence on b.

ORIGINAL PAGE IS
OF POOR QUALITY

ORIGINAL PAGE IS
OF POOR QUALITY

According to /8/ (/11/), separation occurs at F = 0.35 (F = 0.30) if there is a concave pressure distribution present with b<1, and otherwise at F = 0.39 (F = 0.50).
The following table shows the findings at the rear edge for exponential pressure distributions and asymptotic equilibrium distributions with the same rear edge velocity as well as a. equilibrium distributions with constant undisturbed flow and at the same time equal potential difference.

/248

1 Geschwindigkeitsverteilung	u_c/u_∞	u_Δ/u_∞	H32c	$\delta 2c/c^* 100$	F
2 exponentiell b=1/3 (konkav)	0.509	0.662	1.581	0.97	0.39
asympt. Aequilibrium m=-.222	0.509	0.627	1.647	0.89	-
3 Vorlauf und a.Aequi. m=-.237	0.509	0.662	1.597	1.17	-
4 exponentiell b=1.0 (linear)	0.627	0.829	1.559	0.79	0.50
asympt. Aequilibrium m=-.179	0.627	0.731	1.699	0.54	-
3 Vorlauf und a.Aequi. m=-.236	0.627	0.829	1.604	0.85	-
5 exponentiell b=3.0 (konvex)	0.723	0.936	1.501	0.66	0.60
asympt. Aequilibrium m=-.139	0.723	0.807	1.731	0.42	-
3 Vorlauf und a.Aequi. m=-.248	0.723	0.936	1.575	0.68	-

Key: 1 velocity distribution; 2 exponential b = 1/3 (concave); 3 undisturbed flow and a. equlibrium; 4 exponential b = 1.0 (linear); 5 exponential b = 3.0 (convex).

If there is no restriction relative to the maximum velocity, equilibrium distributions are favorable for achieving high thrust forces, as they make a higher pressure increase possible. On the other hand, these distributions do not produce any resistance reduction compared with exponential distributions, as long as the transition point lies in the same place and turbulent separation is avoided. With the same potential difference, which is a criterion for the thrust force in the pressure increase zone, there is even an increase in resistance.

3.3 Velocity optimization

In order for a physically reasonable velocity distribution can be calculated from the form parameter given, first of all there must be an obstruction point at the profile nose, secondly the laminar-turbulent transition should meet a suitable transition criterion, or take place at a pre-determined point as a result of a suitable roughness, and thirdly a pre-determined velocity has to be reached at the rear edge.

Figure 4 shows the way in which the boundary layer-optimized profiles are calculated.

In order to determine the transition point either su, Uu or the form parameter $H32_2$ in the laminar transition zone has to be determined. The transition calculation is done according to Abu-Ghannam /12/ (Fig. 5).

Figure 6 shows the pressure force factors ca for the profile suction side in relation to the resistance factor cw, which was calculated according to Squi e-Young. /249

Modified Stratford equilibrium distribution - (P = 1, P = 1.74),an exponential equilibrium distribution - (b = 1/3, b = 1), and an asymptotic equilibrium distribution (m = -.245) were compared.

The onset of the pressure increase is varied.

The following values were given for the optimization:

$Re_\infty = 10^6$, $Ma_\infty = 0.1$, $Tu_\infty = 4\%$, $H32_1 = 1.625$, $H32_2 = 1.620$, $H32_3 = 1.80$, $H32c = 1.55$, $s1/c = 0.05$, $Uc/U_\infty = 0.9$ (1.1), $st/c = 0.3 + 0.8$ (0.95).

In the case of low ca values, the resistance is almost independent of the velocity distribution.

The following table shows the results for ca = 0.5.

[1] Geschwindigkeitsverteilung	Uc/U	Uu/U	at/c	H32c	cw*100
Stratford P = 1	0.9	1.48	0.611	1.554	0.985
Stratford P = 1.74	0.9	1.67	0.389	1.622	0.936
[2] exponentiell b = 1/3	0.9	1.46	0.610	1.548	0.951
asympt. Aequilibrium m=-.245	0.9	1.49	0.534	1.572	0.964
Stratford P = 1	1.1	1.33	0.940	1.578	0.885
[2] exponentiell b = 1	1.1	1.32	0.914	1.506	0.932

Key: 1 velocity distribution; 2 exponential.

Figure 7 shows the distributions calculated for ca = 0.5. For the low rear edge velocity the mod. Stratford distribution (P = 1.74) is somewhat superior. An increase in the rear edge velocity produces an obvious improvement.
Since the transition point is almost constant, the resistance changes only slightly for a change in the velocity distribution. On the other hand, the separation-free attainable thrust for equilibrium distributions close to separation, or similar distributions, is much greater.

4. Calculation of the profile contour.

The profile form is calculated from the boundary layer-optimized velocity distribution using design methods.
For subsonic flows a computer program was developed with which an initial contour is iteratively improved until the desired velocity /250
distribution is obtained /2/, /5/. In each case only the velocity distribution of one profile side is adjusted. for the iteration, either the profile thickness or the opposite contour is retained. The iteratively used computer program is a panel program of the first magnitude with high calculation exactness.
Figure 8 shows the contour calculation of a profile with a flap for which the underside is retained, and the countour calculation of a double cascade with the division one, for which the profile thickness remains constant and it shows the relevant convergence behavior.

For individual profiles the design program according to /9/ has pro·en useful; it operates with conformal illustration and permits

ORIGINAL PAGE IS
OF POOR QUALITY

pre-determination of the velocity for several angle of attack.

Figure 9 shows a profile with constant velocity ranges for three different angles of attack.
For transsonic flows the design method developed in Project B8 is used. Within Project B8 the contour was calculated for an optimized velocity determination. The velocity distribution was selected in such a way that part of the pressure increase was displaced into the wake (Fig. 10).

5. Non-design state

The non-compressible cascade flow is calculated using a panel method of the first magnitude /1/ which has a degree of exactness as high as conformal illustration, although for a number of profiles it is much simpler to use. For subssonic cascades the effect of compressibility can more or less be attributed to non-compressible flows via a transformation. Good results were obtained using the Karman-Taien Rule.
Figure 11 shows the transformed geometry and the calculated pressure distribution compared with measurement.
In order to calculate the compressible boundary layer an integral method is used /13/. Comparisons with measurements are shown in Fig. 19. In the case of iterative flow the pressure distribution can be calculated using the iteratively applied post-calcualtion method /6/.
Figure 12 shows a comparison between calculation and measurement. /251

6. Calculation of non-stationary flows

The flow through a compressor phase is non-stationary because of the relative movement between the wheel and the guide ring. Taking into account the turbulence trails that occur, any non-stationary flows can be calculated using the panel method.
The time-related thrust, the circulation and the turbulence trail for a beginning cascade, which experineces the initial flow at below 45°, are shown in Fig. 13.

Figure 14 shows for one turbine phase the development of the turbu-

lence trail from the quasi-stationary initial state and the bucket force fluctuation in the circumferential direction in the final state.
Figure 15 shows the turbulence trails that occur when the flow moves around a flat plate with a finite rear edge thickness, and the circulation of the resulting turbulence.

7. Experimental studies

The transsonic cascade wind channel was modified in order to be able to measure compressor cascades also.
In order to avoid any influence on the cascade flow as a result of separation after the sound barrier, which would be possible in an upward flow direction via the wall boundary layer, the transition from the right-angled measurement cross section to the circular cross section was designed to be separation-free and the sound barrier was replaced by suitable wire sieves.
In order to be able to study separated cascade flows interferometrically using laser double illumination holography, the illumination light, which up to now was set at 1/300 second by means of a central shutter, had to be shortened to a few microseconds. This was achieved with the aid of a rotating disc with an adjustable aperture. At the same time the optical design had to be changed so that the intensity of the 1 watt laser was sufficient.
The profiles SKG 1.3 and SKG 2.7 were measured. Separation occurred /252
in the design atate for both profiles. Figure 17 shows the interferogram and the coating picture in the design state.
When the flow Mach number is reduced (Ma $\leqslant$ 0.7) the flow re-attaches, i.e. a laminar separation bubble forms (Fig. 18).
In order to compare loss measurement and boundary layer measurement, the velocity distributions obtained from the interferogram were used for the boundary layer calculation. The degree of turbulence (Tu = 0.2%) was adjusted at the measured

Figure 19 shows the calculated boundary layer development for Ma = 0.7. On the suction and pressure side laminar bubbles are calculated in accordance with the measurement.
Figure 20 shows the measured and calculated pressure loss factor

$\zeta_{13} = (p01 - p03)/(p01-p1)$; p03 is the impulse-related pressure after the cascade.

8. Summary

It was possible in Project B6 to realize the desired objective of transferring the design philosophy for individual profiles to cascades.
The basis of the design is the selection of a form parameter distribution that is adapted to the relevant requirements; this is done according to the same reasoning as the individual profile.

The calculation of the velocity distribution from the form parameter distribution, which has not been carried out in this form before, is valid for individual profiles and cascades when a suitable choice is made for the rear edge velocity.
For the subsequent contour calculation and calculation of the non-design states, reliable computer programs were developed for subsonic flows.
For experimental checking, laser double illumination holography and the transsonic cascade channel were developed further, so that separated flows can also be studied.
For future measurements it is necessary to adjust the degree of turbulence. /253

ORIGINAL PAGE IS
OF POOR QUALITY

9. Literary references

/1/ F.X.Wortmann, L.Goettsching: Profilentwurf fuer Gitter. SFB 85 Arbeits- und Ergebnisbericht 1980 - 81 - 82, TU Stuttgart

/2/ F.X.Wortmann, L.Goettsching: Profilentwurf fuer Gitter. SFB 85 Arbeits- und Ergebnisbericht 1979 - 78 - 77, TU Stuttgart

/3/ F.X.Wortmann: Airfoil synthesis techniques, University Texas-Arlington, 1976

/4/ L.Goettsching: Berechnung grenzschichtoptimierter Geschwindigkeitsverteilungen, Institutsbericht IAG, 1986

/5/ L.Goettsching: Ein iteratives Verfahren zur Optimierung zweidimensionaler Profilkombinationen bei inkompressibler Stroemung, Institutsbericht IAG, 78-14, 1978

/6/ L.Goettsching: Exakte Anwendung der Karman-Tsien Regel zur Berechnung kompressibler Gitter-Unterschallstroemungen, Institutsbericht IAG, 79-9, 1979

ORIGINAL PAGE IS
OF POOR QUALITY

/7/ R.H.Liebeck: On the design of subsonic airfoils for high lift, Report No 6463, Douglas, 1976

/8/ B.S.Stratford: The prediction of seperation of the turbulent boundary layer, JFM 5, 1958

/9/ R.Eppler: Ergebnisse gemeinsamer Anwendung von Grenzschicht- und Profiltheorie, ZFW 9, 1960

/10/ E.Truckenbrodt: Neuere Erkenntnisse ueber die Berechnung von Stroemungsgrenzschichten mittels einfacher Quadraturformeln, Ing.-Arch.43, 1974

/11/ T.Cebeci, A.O.Smith: Analysis of turbulent boundary layers, Academic Press, 1974

/12/ B.Abu-Ghannam, R.Shaw: Natural transition of boundary-layers - The effects of turbulence, pressure gradient and flow history, JMES 22, No 5, 1980

/13/ K.O.Felsch: Turbulente Wandgrenzschichten in zweidimensionaler Stroemung, Mitteilungen d. Inst. f.Stroemungsl. u. -maschinen, TH Karlsruhe, No 13, 1972

Key to references:

/1/ F.X.Wortmann, L. Goettsching: Profile design for cascades. SFB 85 Study and Findings Report, 1980-81-82, TU Stuttgart.

/2/ F.X.Wortmann, L. Goettsching: Profile design for cascades. SFB 85 Study and Findings Report, 1979-78-77, TU Stuttgart.

/4/ L. Goettsching: Calculation of boundary layer -optimized velocity distributions. IAG Institute Report. 1986.

/5/ L. Goettsching: An iterative method for optimizing two-dimensional profile combinations for non-compressible flow. IAG Institute Report, 78-14, 1978.

/6/ L. Goettsching: Exact application of the Karman-Tsien Rule for calculating compressible cascade subsonic flows. IAG Institute Report, 79-9, 1979.

/9/ R. Eppler: Results of mutual application of boundary layer and profile theory. ZFW 9, 1960.

/10/ E. Truckenbrodt: New information on the calculation of flow boundary layers using simple quadrature formulae. Ing-Arch. 43, 1974.

/13/ Turbulent wall boundary layers in two-dimensional flow, Reports from the Inst. for Flow Research, TH Karlsruhe, no. 13, 1972.

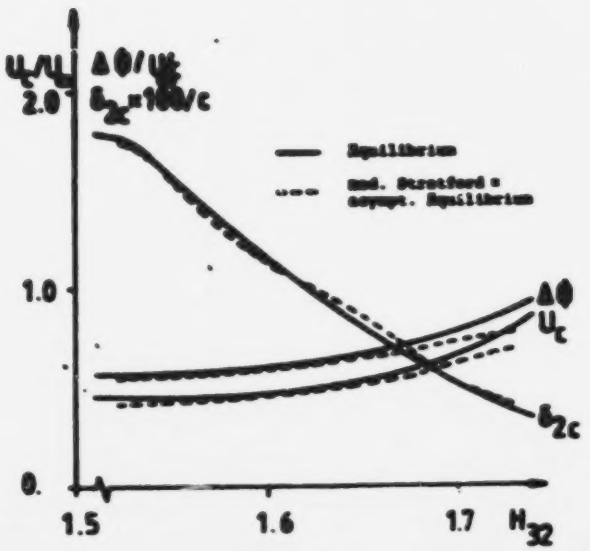

Fig. 1: Comparison of rear edge velocity, impulse loss density and potential difference as functions of the rear edge form parameter for equilibrium, modified Stratford and asymptotic equilibrium distributions.

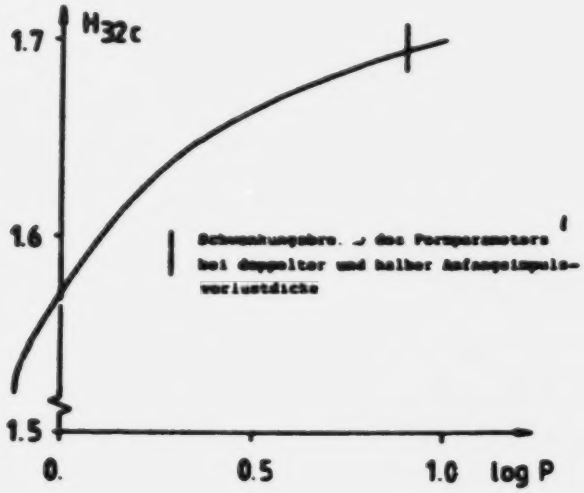

Fig. 2: Rear edge form parameter in relation to modification parameter P for Stratford distributions.

Key: 1 Fluctuation [ill] of the form parameter for double and half initial impulse loss density.

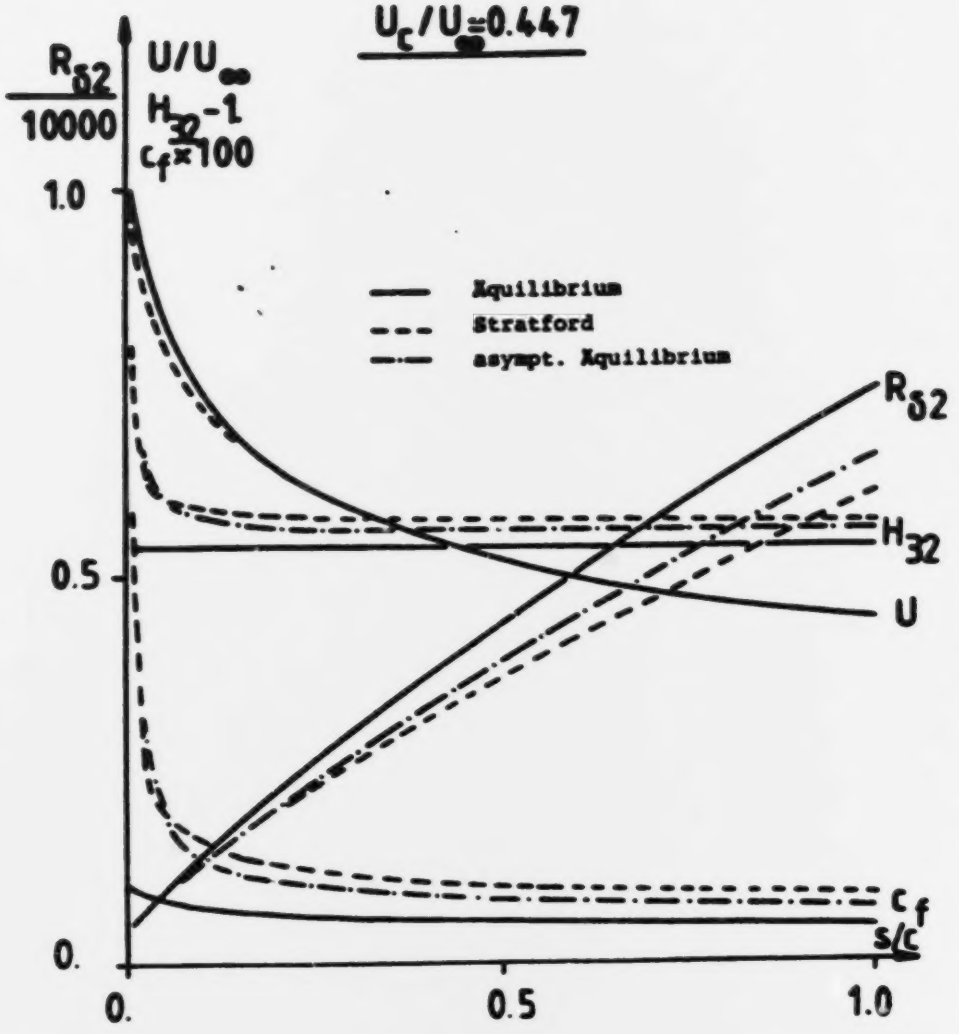

Fig. 3: Comparison of the boundary layer development for Stratford, equilibrium and asymptotic equilibrium distributions.

ORIGINAL PAGE IS
OF POOR QUALITY

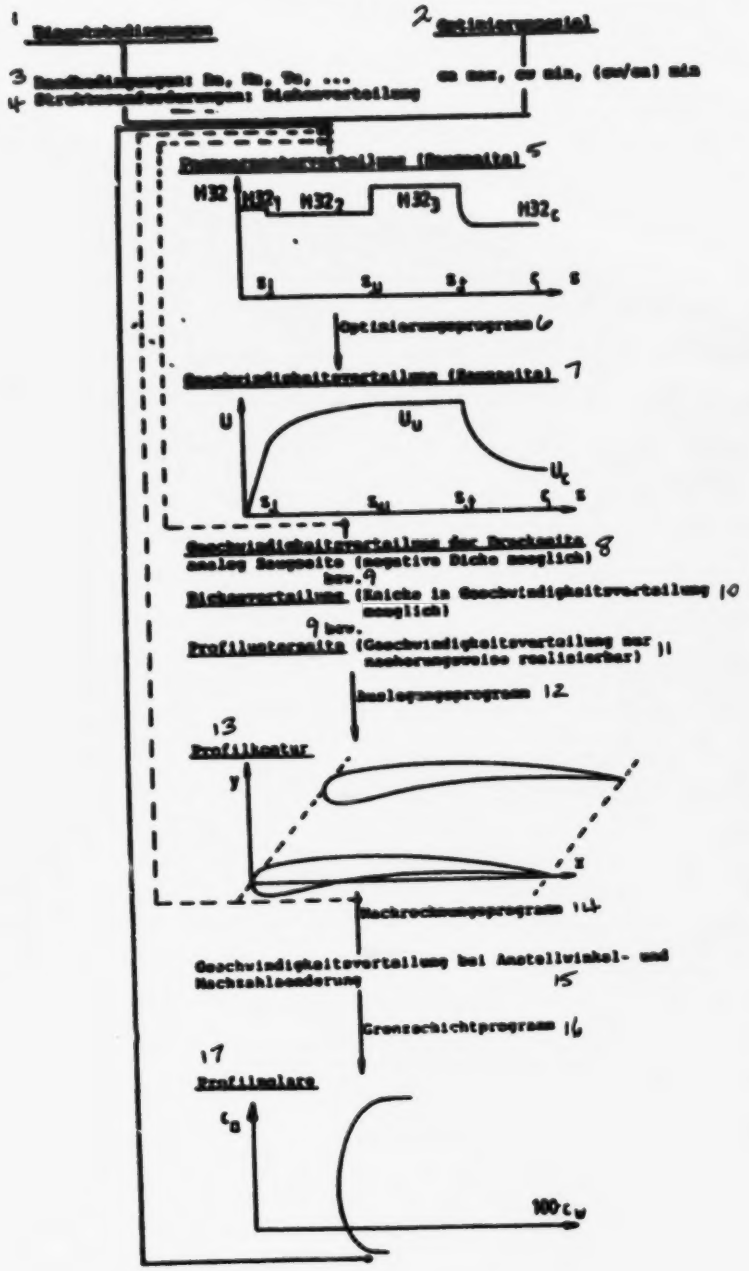

Key: /256

1 use conditions;
2 optimization goal;
3 peripheral conditions;
4 structural requirements: density distribution;
5 form parameter distribution (suction side);
6 optimization program;
7 velocity distribution (suction side);
8 velocity distribution on pressure side: same as suction side (negative density possible);
9 or
10 density distribution (bend in velocity distribution possible);
11 profile underside (velocity distribution can be realized only approx.;
12 design program;
13 profile contour;
14 follow-up calculation program;
15 velocity distribution for change in angle of attack and post-number;
16 boundary layer program;
17 profile polars.

Fig. 4: Calculation of boundary layer-optimized profiles

ORIGINAL PAGE IS
OF POOR QUALITY

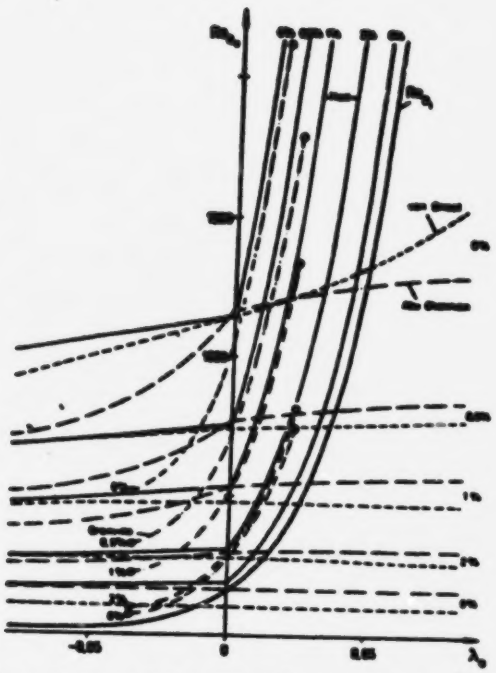

Fig. 5: Transition Reynolds no. $Re_{\theta u}$ in relation to form parameter and degree of turbulence acc. to various authors.

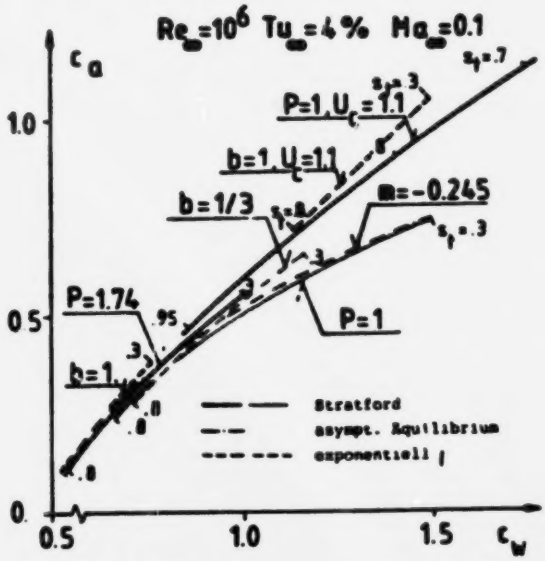

Fig. 6: Profile polars for variation of onset of pressure increase ($S_t/C = 0.3 \div 0.8$) for exponential (P = 1/3, P = 1), Stratford (P = 1, P = 1.74) and asymptotic equilibrium distributions (m = -0.245). [Key: 1 exponential].

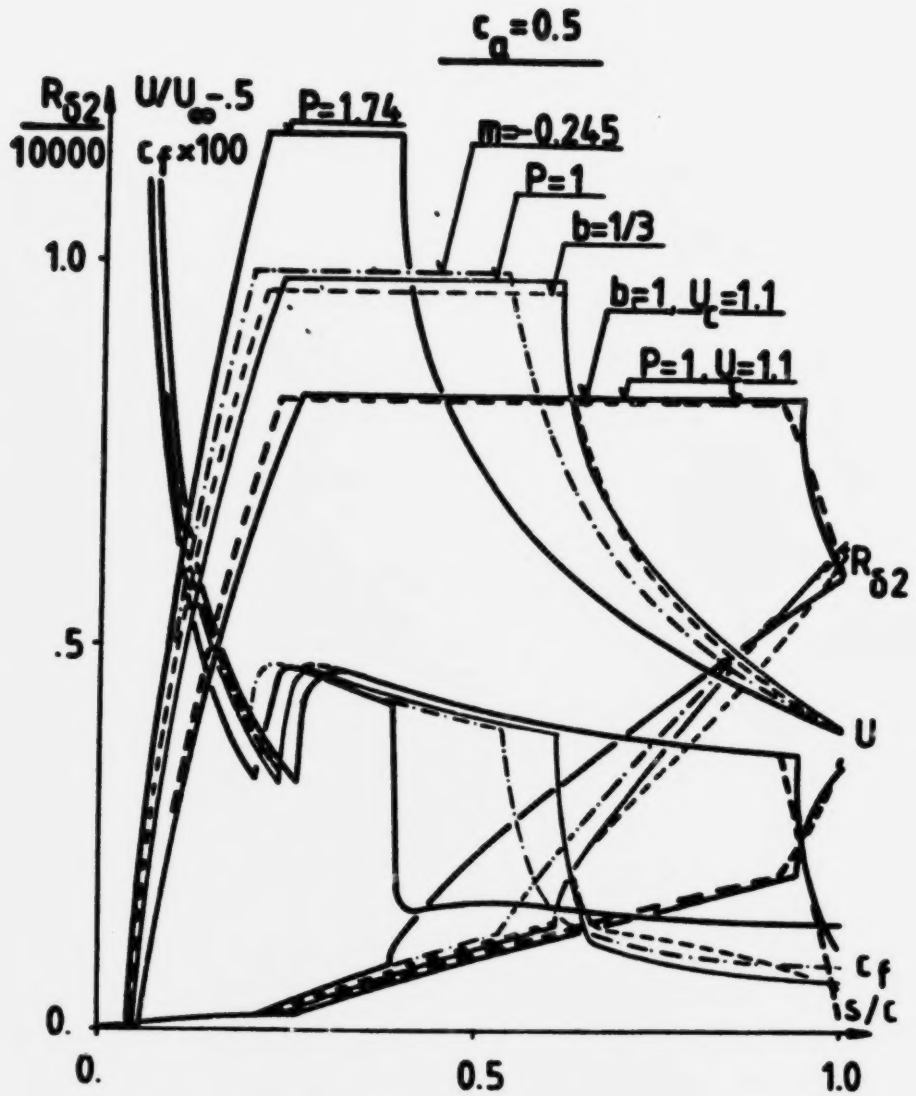

Fig. 7: Velocity distribution and boundary layer development for the case c_a = 0.5 for exponential (b = 1/3, b = 1), Stratford (P = 1, P = 1.74) and asymptotic equilibrium distributions (m = -0.245).

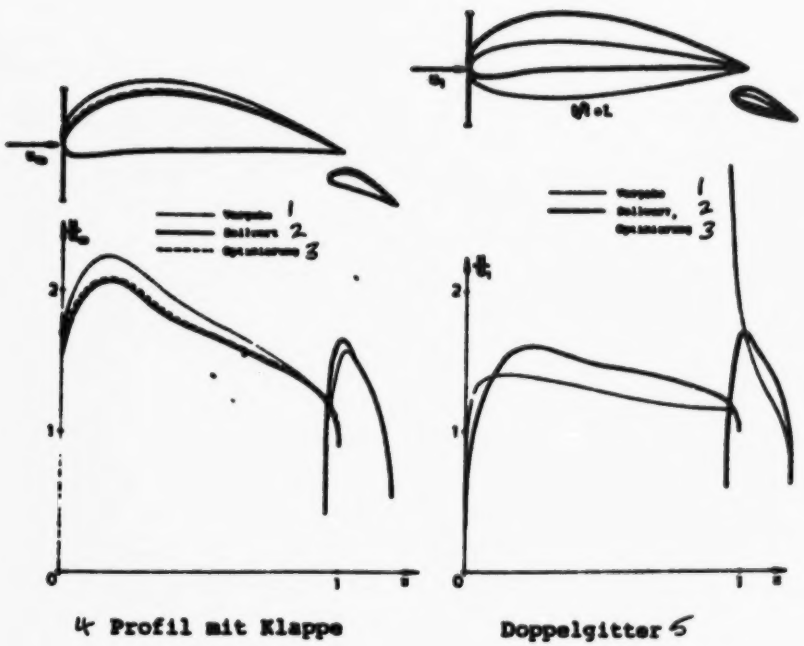

4 Profil mit Klappe

Doppelgitter 5

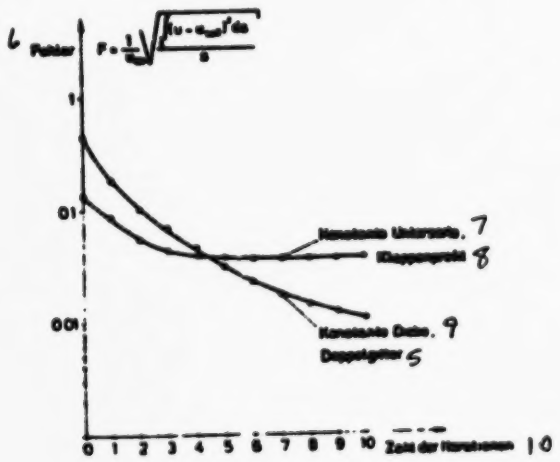

Fig. 8: Calculation of contour of profile with flap and with fixed underside, and calculation of double cascade for fixed profile density and appropriate convergence behavior.

Key: 1 predetermined; 2 factor; 3 optimization; 4 profile with flap; 5 double cascade; 6 error; 7 constant underside; 8 flap profile; 9 constant density; 10 no. of [ill.].

ORIGINAL PAGE IS
OF POOR QUALITY

CHARACTERISTIC
CE BOOK QUALITY

/260

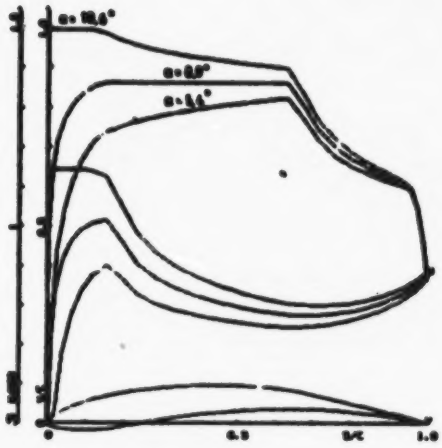

Fig. 9: Example of contour calculation using conformal illustration for an individual profile.

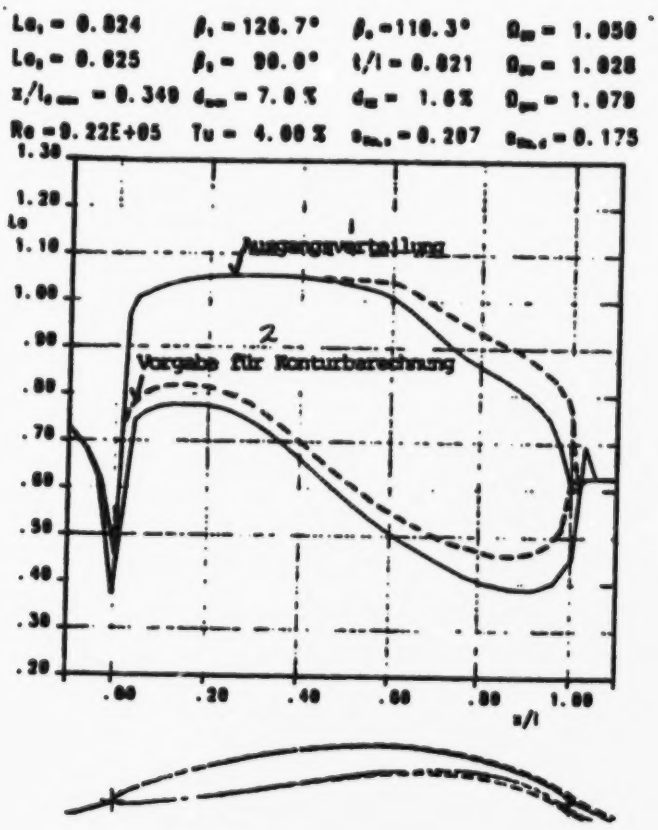
Ma₁ = 0.824 β₁ = 126.7° β₂ = 118.3° Θ = 1.050
Ma₂ = 0.825 β₂ = 90.0° t/l = 0.821 Θ = 1.028
x/l = 0.348 d = 7.8 % d = 1.6 % Θ = 1.079
Re = 0.22E+06 Tu = 4.00 % δ* = 0.207 δ** = 0.175
Ma
Ausgangsverteilung
2
Vorgabe für Konturberechnung
x/l

Fig. 10: Velocity predetermination for super-critical compressor cascade ($Ma_1 = 0.8$, $Re_\infty = 10^6$, $Tu_\infty = 4\%$) and relevant contour.

Key: 1 initial distribution; 2 predetermination of contour calculation.

ORIGINAL PAGE IS
OF POOR QUALITY

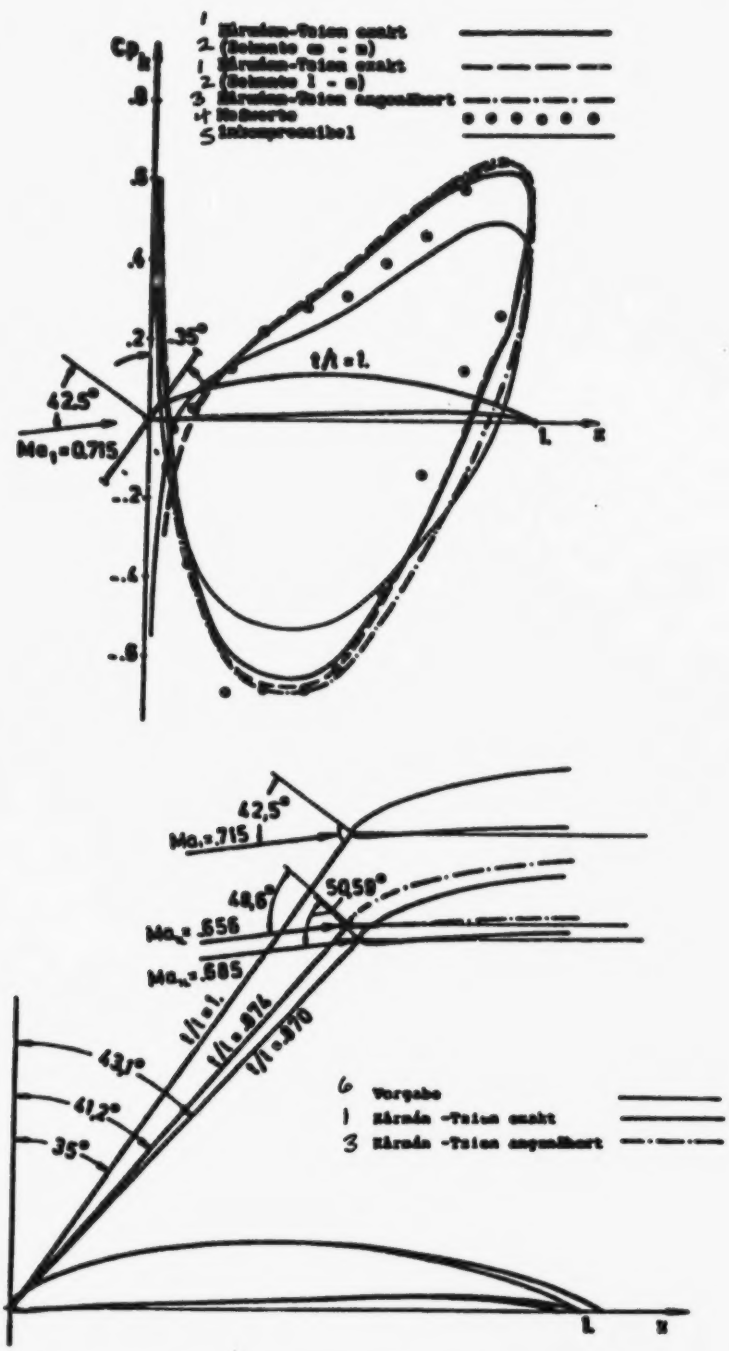

Fig. 11: Pressure distribution and transformed geometry for NACA 65-(12 A_{10}). 10 profiles in cascade group for flow Mach no. Ma_1 = 0.715.

Key: 1 Karmann-Tsien, exact; 2 secant; 3 Karmann-Tsien, approx.; 4 measurement values; 5 non-compressible; 6 predetermined.

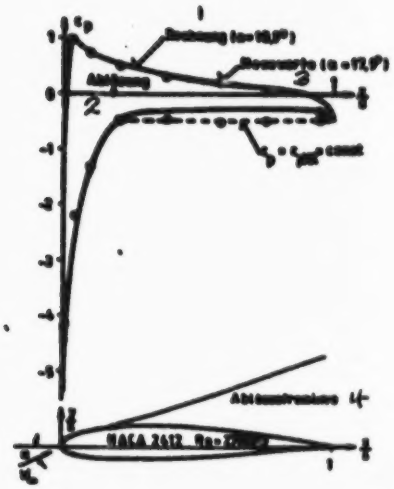

Fig. 12: Pressure distribution for separated flow. Comparison between calculation and measurement.

Key: 1 calculation; 2 separation; 3 measurement values; 4 separation dividing line.

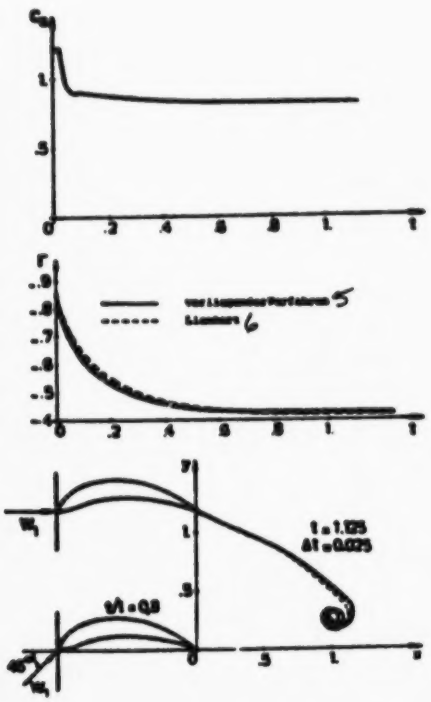

Fig. 13: Thrust, circulation and turbulence trail geometry for start-up of cascade (Betz-Keune profile) for flow below 45°.

Key: 5 current method;
6 [ill.]

ORIGINAL PAGE IS
OF POOR QUALITY

ORIGINAL PAGE IS
OE POOR QUALITY

/263

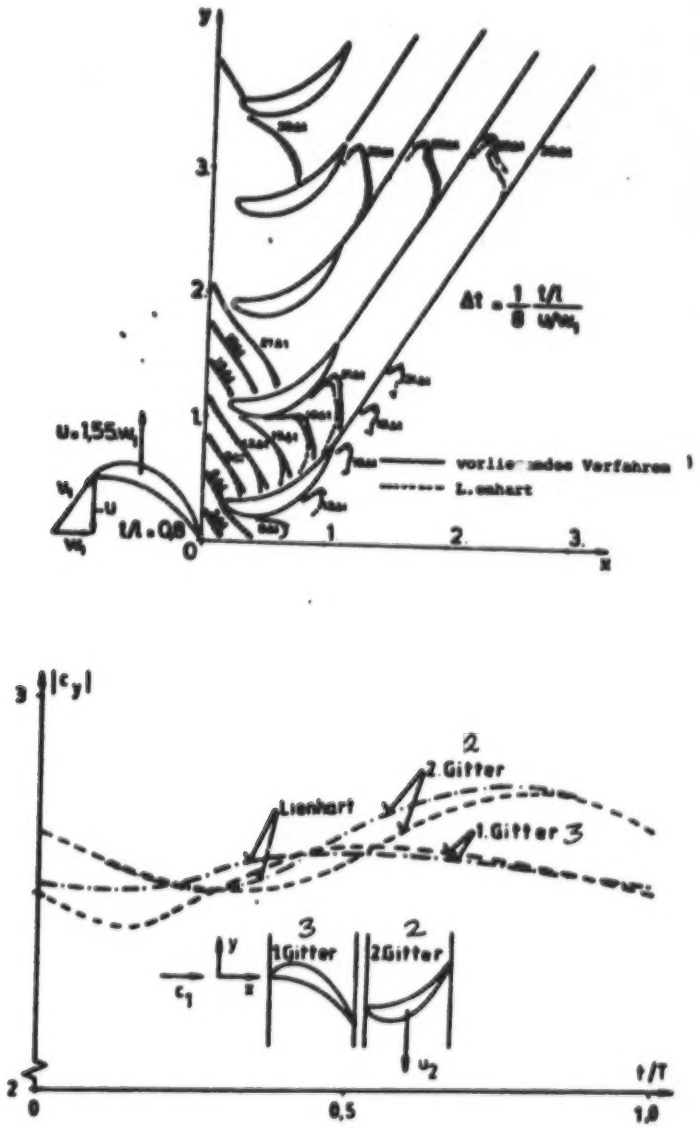

Fig. 14: Onset of turbulence trail development from quasi-stationary state and circumferential force fluctuation over a period.

Key: 1 current method; 2 2nd. cascade; 3 1st. cascade.

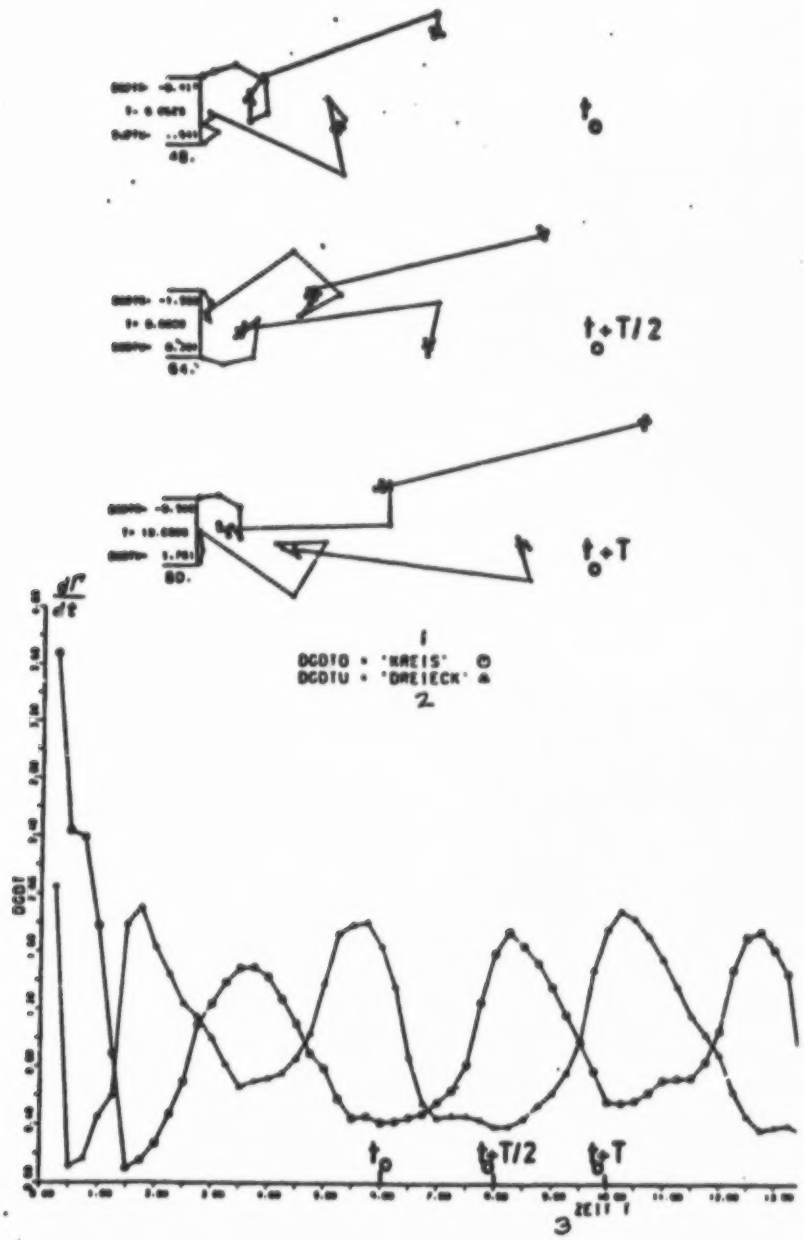

Fig. 15: Geometry of turbulence trails and time-related change in trail circulation for flat plate of finite thickness.

Key: 1 circle; 2 triangle; 3 time.

ORIGINAL PAGE IS
OF POOR QUALITY

ORIGINAL PAGE IS
OF POOR QUALITY

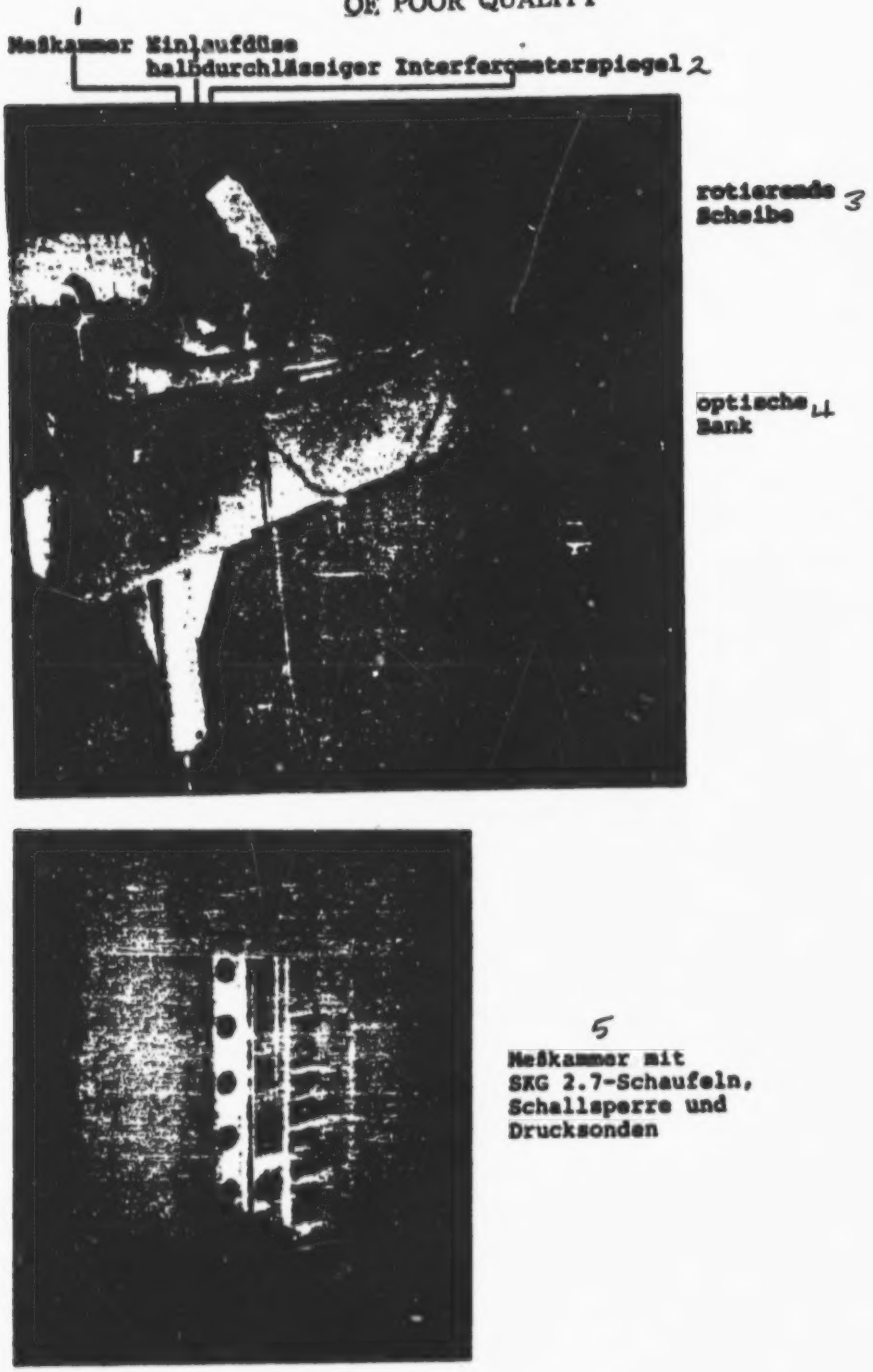

Fig. 16: Test set-up.

Key: 1 measurement chamber inlet jet; 2 semi-permeable interferometer mirror; 3 rotating disc; 4 optical bank; 5 measurement chamber with SKG 2.7 buckets, sound barrier and pressure probes.

ORIGINAL PAGE IS
OF POOR QUALITY

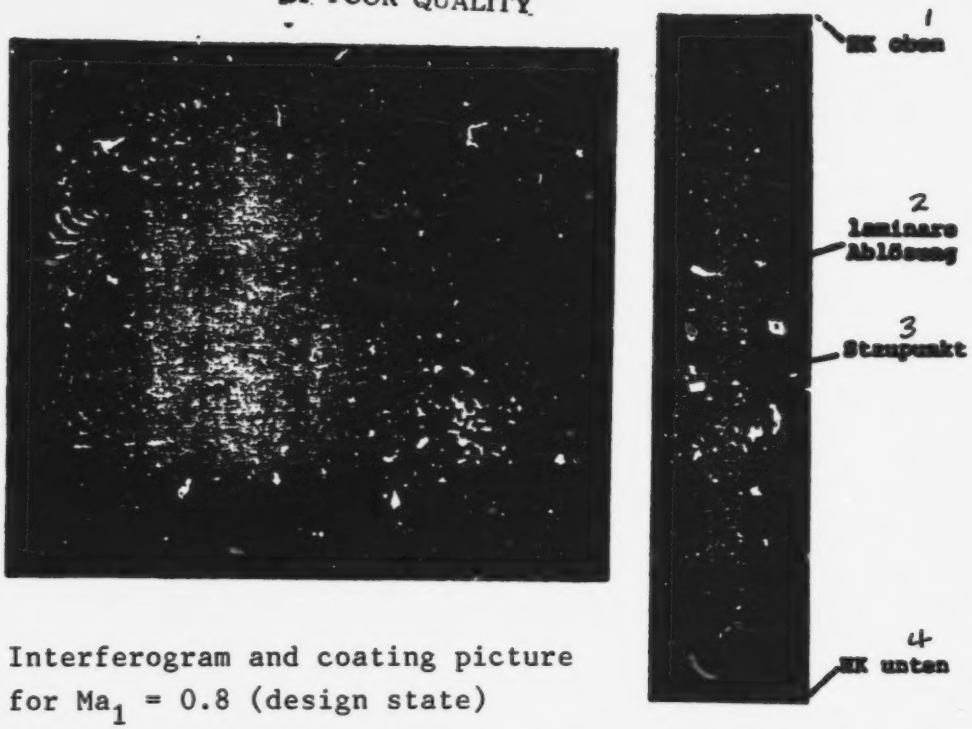

Fig. 17: Interferogram and coating picture for $Ma_1 = 0.8$ (design state)

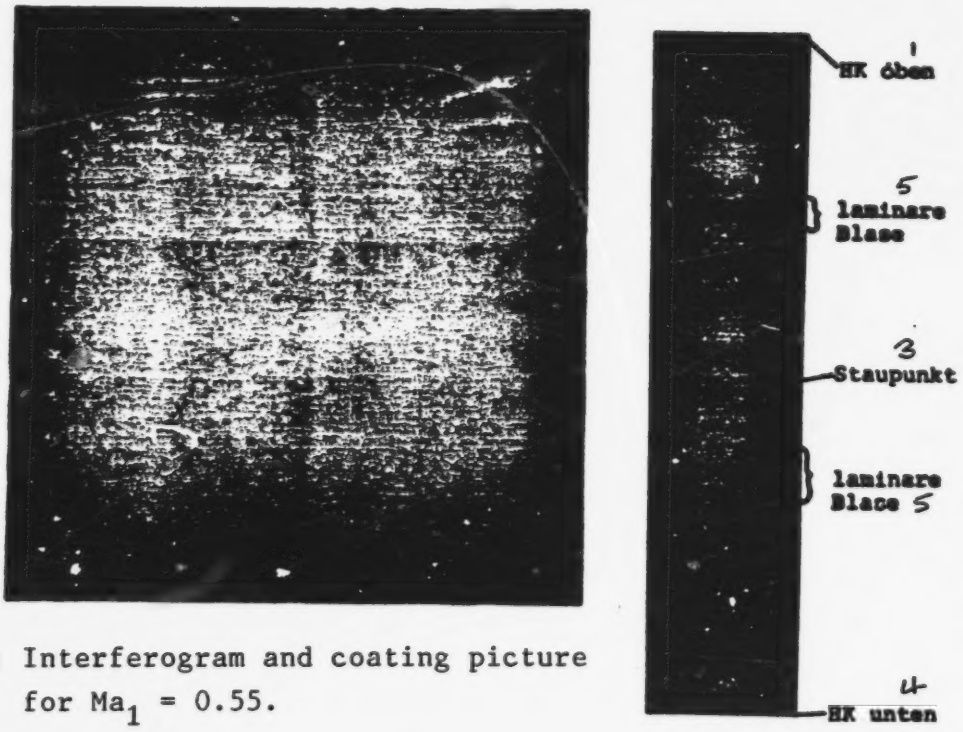

Fig. 18: Interferogram and coating picture for $Ma_1 = 0.55$.

Key: 1 top; 2 laminar separation; 3 obstruction point; 4 bottom; 5 laminar bubble.

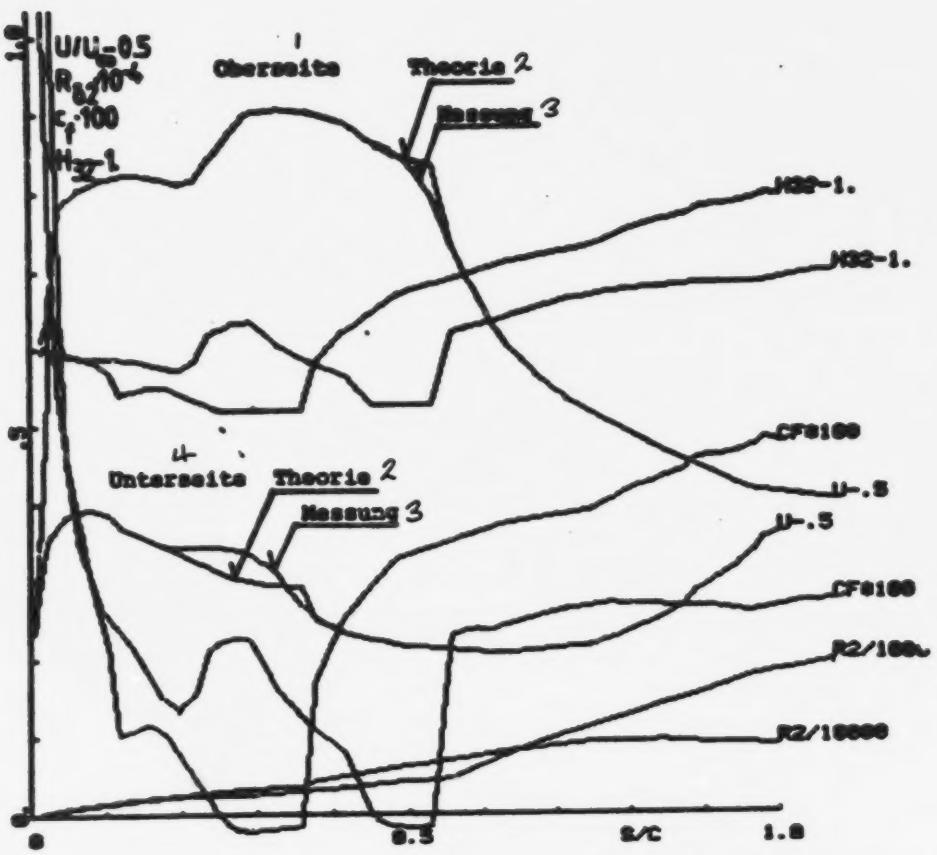

Fig. 19: Boundary layer development on SKG 2.7 profile for predetermination of measured velocity distribution (with exception of bubble zone) for $Ma_1 = 0.7$.

Key: 1 upper side; 2 theory ; 3 measurement; 4 underside.

ORIGINAL PAGE IS
OF POOR QUALITY

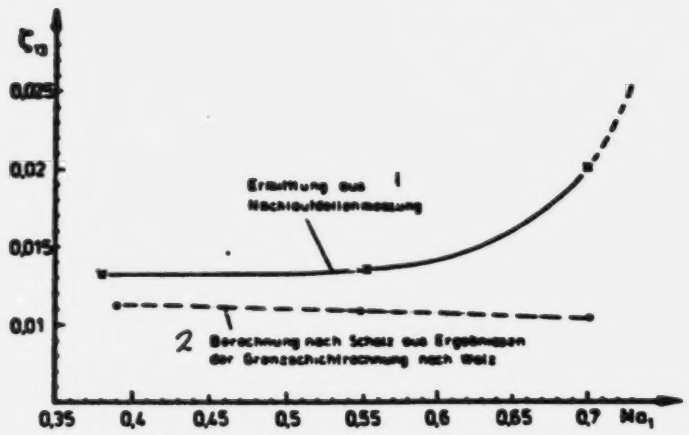

Fig. 20 : Comparison between theory and measurement of pressure loss factors for SKG 2.7 profile.

Key; 1 obtained from wake indentation measurement; 2 calculated acc. to Scholz from findings from boundary layer calculation acc. to Walz.

ORIGINAL PAGE IS
OE POOR QUALITY